Batteries & Supercaps

Research Article
doi.org/10.1002/batt.202500066

Chemistry Europe
European Chemical Societies Publishing

www.batteries-supercaps.org

Siloxane-Based Polymer Gel Electrolytes for Sodium Metal Batteries with Long Lifespan at High Rates and Low Temperatures

Yu Xie,[a] Dafeng Wei,[a] Junqiao Huang,[a] Zhichuan Shen,[a] Mengxue Wu,[a] Xuan Ye,[a] Zekai Chen,[a] Song Xiao,[a] Jianwei Chen,[a] Abdullah N. Alodhayb,[b] Ping Chen,[c, d] and Zhicong Shi*[a]

To address the scarcity of lithium metal resources and the leakage issues associated with traditional liquid batteries, the development of solid-state sodium metal batteries (SMBs) is necessary. However, the advancement of solid SMBs has been significantly impeded by the low ionic conductivity of solid electrolytes and poor electrode compatibility. To overcome these challenges, this study employs an in-situ polymerization method to synthesize a gel polymer electrolyte, by incorporating 3-(Trimethoxysilyl)propyl methacrylate (TPM) into the polymer network. When 5% TPM is added, the room-temperature ionic conductivity and sodium-ion transference number of GPE are notably enhanced to 4.54×10^{-2} S cm^{-1} and 0.58, respectively, with an oxidation voltage reaching 4.59 V. Due to the formation of a dense SEI film rich in F and Cl on the surface of sodium metal, the sodium symmetric batteries using GPE-TPM-5 can work stably for more than 3200 h at the current density of 0.1 mA cm^{-2}. The NVP|GPE-TPM-5|Na batteries exhibit excellent cycle life of over 15000 cycles at a rate of 10 C, with a capacity retention rate of 91%. It also demonstrates more than 800 cycles with a capacity retention rate of 94% at −20 °C and 1C. This research provides a new approach for preparing gel polymer electrolytes for SMBs with superior long-term cycling performance at a high rate and a low temperature.

1. Introduction

In light of the current shortage of fossil fuels, electrochemical energy storage has garnered significant attention.[1–3] Compared to lithium metal batteries (LMBs), sodium metal batteries (SMBs) offer a distinct advantage due to the higher natural abundance and wider distribution of sodium elements, resulting in lower production costs and promoting sustainable development.[4–7] Despite having properties similar to LMBs, SMBs face challenges due to the slower kinetics caused by the larger ionic radius of Na^+, which is a critical issue that needs to be addressed for the advancement of SMBs.[8]

Another critical concern pertains to the safety of batteries that commonly employ liquid electrolytes (LE). During battery operation, heat generation can lead to a rise in internal temperature. This increase may cause the organic solvents within the liquid electrolyte to vaporize, resulting in a rapid escalation of internal pressure and potentially spontaneous combustion.[9] Moreover, liquid electrolytes are susceptible to leakage. Under complex conditions, battery damage is inevitable, which poses a significant risk of LE leakage and consequently more severe accidents. To address the aforementioned challenges, the concept of solid-state electrolytes (SSEs) has been introduced. Solid-state electrolytes effectively mitigate issues related to battery leakage[10] and exhibit superior puncture resistance due to their high mechanical strength, which significantly suppresses dendrite formation.[11,12] However, in practical applications, the inadequate compatibility between SSEs and electrodes/electrolytes hinders ion conduction within the battery[13] thereby impacting its overall performance. Therefore, researchers initiated the investigation of gel polymer electrolytes (GPEs). Unlike traditional LEs, GPEs are synthesized by employing polymers as the backbone carriers and incorporating liquid electrolytes. By precisely controlling the polymer matrix, the incorporation of liquid electrolyte can exceed 90%. This high loading of liquid electrolyte enables GPEs to exhibit electrochemical properties comparable to those of LEs,[14] while the polymer framework ensures the macroscopic stability of the electrolyte. Consequently, GPEs effectively address issues such as leakage of LEs and dendrite growth inhibition.[15] On this foundation, the application of in-situ polymerization technology can significantly augment the advantages of GPEs. In-situ polymerization significantly enhances the properties of the electrode/electrolyte interface by ensuring complete impregnation of the electrode with the polymer precursor solution, followed by its conversion into a polymer. This process

[a] Y. Xie, D. Wei, J. Huang, Z. Shen, M. Wu, X. Ye, Z. Chen, S. Xiao, J. Chen, Z. Shi
Institute of Batteries, School of Materials and Energy, Guangdong University of Technology, Guangzhou, 510006, China
E-mail: zhicong@gdut.edu.cn

[b] A. N. Alodhayb
Department of Physics and Astronomy, College of Science, King Saud University, Riyadh, 11451, Saudi Arabia

[c] P. Chen
BST Power (Shenzhen) Limited, Shenzhen 518000, China

[d] P. Chen
Hengyang BST Power Limited, Hengyang 421000, China

Supporting information for this article is available on the WWW under https://doi.org/10.1002/batt.202500066

guarantees optimal contact between the electrode and the gel electrolyte.[16]

However, the issues associated with GPE are evident, despite their high liquid component content, as they exhibit significantly lower conductivity and ion transport efficiency compared to LE. This phenomenon is attributed to the reduced transport efficiency of ions within the polymer matrix relative to the liquid phase. To address this challenge, the utilization of siloxane-based organics has been proposed, owing to their enhanced chain flexibility and segmental mobility.[17] Additionally, polysiloxane possess superior oxidation resistance and thermal stability.[18] Moreover, polysiloxane generally possess a lower glass transition temperature (T_g), which facilitates an increased segmental motion.[19] This enhanced mobility can improve charge transport, thereby contributing to the improved low-temperature performance of SMBs.

In this study, we designed a copolymer using poly(ethylene glycol) diacrylate (PEGDA) and bisphenol A ethoxylate diacrylate (BPAE) as monomers, incorporating 3-(Trimethoxysilyl)propyl methacrylate (TPM) as an additive to form the polymer backbone (Figure 1). This GPE was synthesized via in-situ polymerization. The three selected substances contain ester groups, and the presence of a significant number of these groups facilitates the dissociation of sodium salts and restrict the movements of anions during the operation of battery.[20–22] Moreover, ester polymers exhibit higher oxidation voltages compared to polyethers, which helps mitigate side reactions between the cathode and electrolyte when voltage is increased.[23,24] Due to the introduction of TPM, the prepared GPE demonstrated superior ionic conductivity and migration efficiency, thereby extending the operational lifespan of the battery. This approach offers a novel strategy for researching the sodium ion gel electrolytes.

Experimental Section

Materials

Poly(ethylene glycol) diacrylate (PEGDA), Bisphenol A ethoxylate diacrylate (BPAE), 2,2′-Azobis(2-methylpropionitrile) (AIBN) were purchased from Macklin Corporation. N-methyl-pyrrolidone (NMP), 3-(Trimethoxysilyl)propyl methacrylate (TPM) were obtained from Aladdin Corporation. $Na_3V_2(PO_4)_3$ powder (NVP) and acetylene black were purchased from Guangdong Canrd New Energy Technology Co., Ltd. Liquid electrolyte (NC-061) with $NaClO_4$ in PC:EC = 2:1 (v/v) was provided by DodoChem Co., Ltd. All materials were used without further purification.

Preparation of Cathodes

NVP powder, acetylene black and polyvinylidene fluoride (PVDF) were mixed together in the ratio of 8:1:1 to obtain the homogeneous slurry. The slurry was then evenly coated on an aluminium foil, and dried at 120 °C for 12 h under vacuum. The aluminium foil was cut in the form of a circular sheet of 10 mm diameter. The mass loading of NVP active material is 1 mg cm^{-2}.

In-situ Preparation of Gel Polymer Electrolytes and SMBs

The preparation of the gel electrolyte and the assembly of the sodium metal battery were conducted in an argon-filled glovebox. Initially, PEGDA and BPEA were mixed at a mass ratio of 5:1. Subsequently, varying amounts of TPM (0%, 1%, 5%, and 10% by mass) were added to this mixture. The resulting blend was then combined with the electrolyte solution at a mass ratio of 1:19, named GPE and GPE-TPM-X (X = 1,5,10). After thorough mixing for one hour, the mixed precursor solution was obtained. During the battery assembly, the precursor solution was injected into the glass fiber separator. The dosage of the precursor solution is set at 120 μL, which has been carefully determined to ensure the electrolyte sufficient to completely fill the internal volume of the battery. After which the battery was placed in an oven maintained at 60 °C for 300 minutes to complete the formation of the sodium metal batteries.

Materials Characterization

The X-ray diffractometer (XRD) was used for the analysis of the crystalline morphology of GPE (Bruker AXS GmbH, Karlsruhe, Germany). Scanning electron microscopy (SEM) was used to observe the surface morphology of GPE and the sodium metal negative electrode (Hitachi, Tokyo, Japan). Energy dispersive spectrometer (EDS) was employed to analyze the elemental distribution on the sodium metal surface. Thermogravimetric analyzer (TGA) was applied to assess the thermal stability of GPE

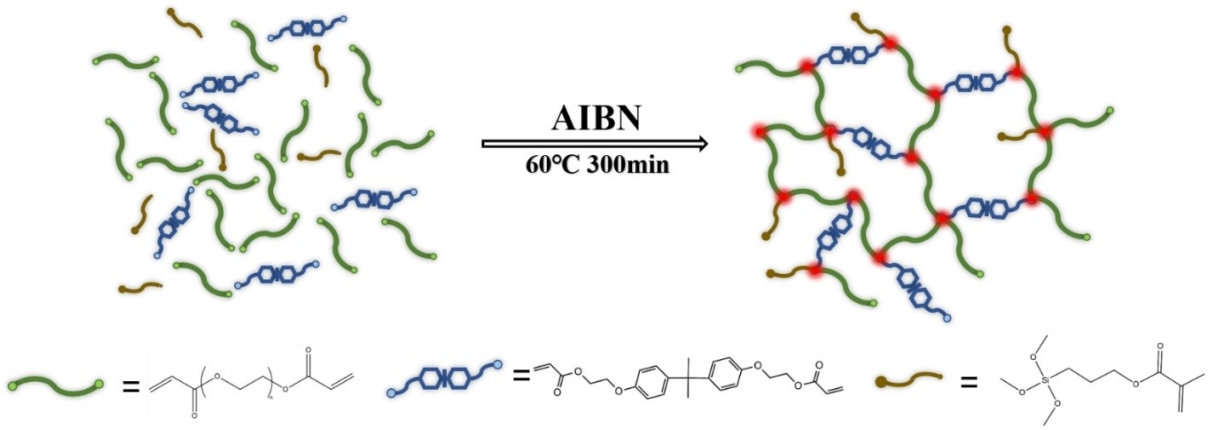

Figure 1. Polymerization process of GPE.

Research Article
doi.org/10.1002/batt.202500066
Chemistry Europe
European Chemical Societies Publishing

(Mettler-Toledo, Columbus, OH, USA). Fourier transform infrared spectroscopy (FTIR) and Raman spectroscopy were employed to analyze the composition of GPE within the wave number ranges of 2500~500 cm^{-1} and 350~1150 cm^{-1}, respectively (Perkin-Elmer, Waltham, MA, USA).

Electrochemical Characterization

Electrochemical impedance spectroscopy (EIS) was carried out using a ZIVE SP1 electrochemical workstation (Shanghai Anzinc). The ionic conductivity(σ) of GPE was tested by EIS using symmetric batteries with stainless steel (SS) as electrode, in the temperature range from 30 °C to 90 °C at certain frequency range from 10^6 to 0.05 Hz. The ionic conductivity is calculated based on the following formula:

$$\sigma = \frac{I}{R_s S}$$

where I represents the thickness of the GPE, R_s is the resistance of the GPE, and S stands for the geometric area of the SS electrodes.

The sodium-ion transference number (t_{Na}^+) of the GPE was evaluated by using a combination of EIS and DC polarization chronoamperometry measurements. t_{Na}^+ can be calculated via the equation of:

$$t_{Na}^{+} = \frac{I_s\ (\Delta V - I_0 R_0)}{I_0\ (\Delta V - I_s R_s)}$$

where I_0 and I_s are initial current and steady-state current, respectively, R_0 and R_s represent initial resistance and steady-state resistance, respectively, ΔV is the applied disturbance voltage (10 mV).

Linear sweep voltammograms (LSV) were conducted at a scanning rate of 1 mV s^{-1} from 0 V to 6 V. Cyclic voltammetry (CV) measurements of the NVP|GPE-TPM-5|Na and NVP|GPE|Na batteries were performed at a scanning rate of 0.1 mV s^{-1} from 2.2 V to 3.8 V. To probe sodium deposition and stripping, the assembled sodium symmetric batteries were tested at current densities of 0.1 mA cm^{-2} and 0.25 mA cm^{-2}. A well-designed system (LANHE CT2001A, China) was used to test the constant-current charging and discharging performance of the batteries.

2. Results and Discussion

The polymerized electrolyte is capable of maintaining a gel-like form instead of a mobile liquid state. The transport of Na^+ in GPE and GPE-TPM-X primarily relies on the motion of the C–O–C within the polymer chain segments and C=O in the polymer and LE.[25,26] The morphologies of glass fiber (GF) and GPE were observed by SEM. As illustrated in Figure 2a, GF comprises numerous randomly distributed nanofiber structures that interconnect to form the porous architecture. This structure facilitates continuous transmission channels for Na^+ within the SMBs.[27] After polymerization (Figure 2b), the pores within the GF are infiltrated with the polymer electrolyte, providing a medium that facilitates the uniform distribution and transport of Na^+. This contributes positively to the formation of a dendrite-free electrode surface.[28,29] Figure 2c, d show digital images of the GPE-TPM-5 precursor solution before and after polymerization. The precursor solution is polymerized at 60 °C for 300 minutes, resulting in a transparent gel wherein the liquid electrolytes is retained within the polymer network.

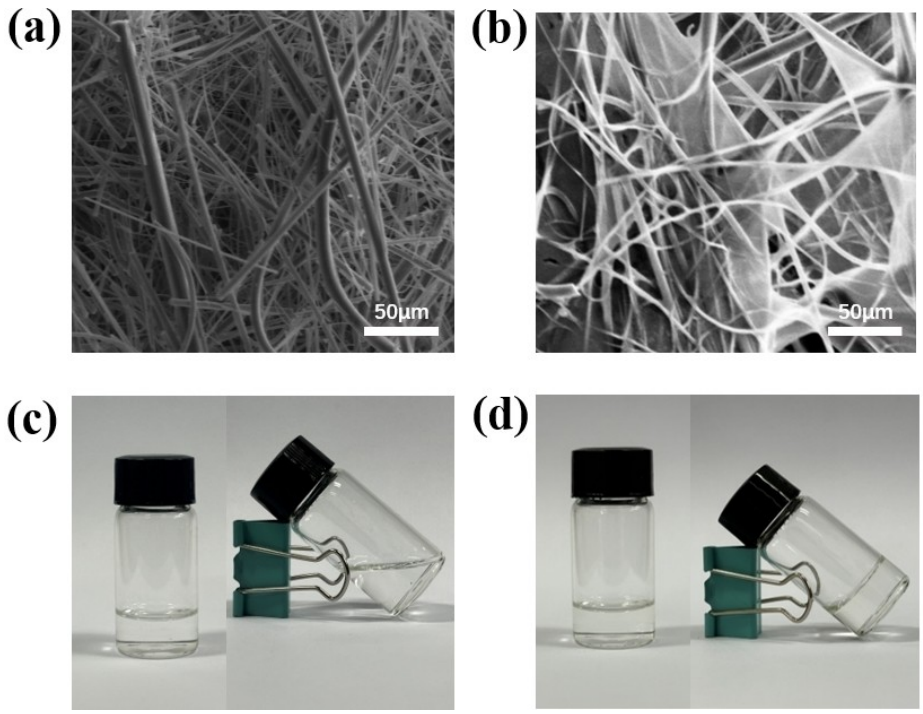

Figure 2. SEM images of (a) Glass fiber separator and (b) Glass fiber with GPE-TPM-5 after polymerization. Digital photographs of GPE-TPM-5 precursor solution (c) before and (d) after polymerization.

Research Article
doi.org/10.1002/batt.202500066
Chemistry Europe
European Chemical Societies Publishing

Figure 3a shows the XRD patterns of GF, GPE and GPE-TPM-5. It is evident that a broad diffraction peak appears in GF at approximately 26°, indicating the presence of a large amount of amorphous phase structure within GF. Following the addition of the polymer, a diffraction peak emerges at approximately 20.54°, signifying the formation of partial crystalline structures within the polymer electrolyte. Appropriate crystallinity is beneficial for maintaining the skeletal structure of the polymer, thereby ensuring that the electrolyte possesses adequate mechanical strength.[12] In particular, it should be noted that the peak pattern in the spectrum of GPE-TPM-5 exhibits a characteristic "steamed bread" peak. This observation suggests that GPE-TPM-5 contains a significant amount of amorphous phase structures and low crystallinity. These amorphous regions facilitate the mobility of polymer chain segments and serve as carriers for Na^+.[30] The enhanced transport of Na^+ is crucial for ensuring high ionic conductivity.[31]

Figure 3b illustrates the FTIR spectra of the individual components of GPE. The wave numbers at 1080 cm^{-1}, 1633 cm^{-1}, and 1755 cm^{-1} correspond to the vibration absorption peaks of Si–O, C=C, and the C=O in ester groups, respectively.[32–34] Following polymerization, the intensity of the C=C bond peaks diminishes, suggesting that free radical polymerization of carbon-carbon double bond breakage can occur between monomers.[35] The C=O peak at 1771 cm^{-1} observed in GPE and GPE-TPM-5 originates from EC in NC-061. The shift in this peak can be attributed to the formation of a coordination between Na^+ and C=O. Additionally, the Si–O peak from TPM overlaps with the C–O–C peak from the liquid electrolyte, but the peak at 963 cm^{-1} for GPE-TPM-5 may represent that an increase in Si–O–Si bonds, suggesting that polymerization between siloxanyl groups may occur during the polymerization process.[36,37]

The Raman spectrum of GPE-TPM-5, with a Raman shift ranging from 350 cm^{-1} to 1150 cm^{-1} (after smoothing), is presented in Figure 3c. Figure S1 provides a comparative analysis of the Raman spectra between GPE-TPM-5 and GPE. The peaks at 954 cm^{-1} and 1083 cm^{-1} correspond to the vibrational characteristics of Si–O bonds in TPM,[38] while the peaks at 439 and 782 cm^{-1} are attributed to the bending vibration of O in Si–O–Si and the symmetric stretching vibration of Si–O–Si, respectively.[39–41] These findings are consistent with the FTIR results, confirming the successful incorporation of TPM into the main chain and indicating the presence of chemical crosslinking.

The thermal stability of GPE and GPE-TPM-5 was evaluated using thermogravimetric analyzer (Figure 3d). The curve of GPE-TPM-5 indicates a slight but gradual mass loss starting from 30 to 100 °C, which can be attributed to the evaporation of residual water in the polymer electrolyte.[42] The mass loss observed between 310~360 °C is associated with the decarboxylation of ester groups within the polymer structure, while the mass loss in the range of 370~500 °C is due to the cleavage of C–O–C bonds.[43,44] For GPE, the rapid mass attenuation observed at 130 °C is attributed to the volatilization of LE. However, this phenomenon occurs at 185 °C for GPE-TPM-5. After polymer-

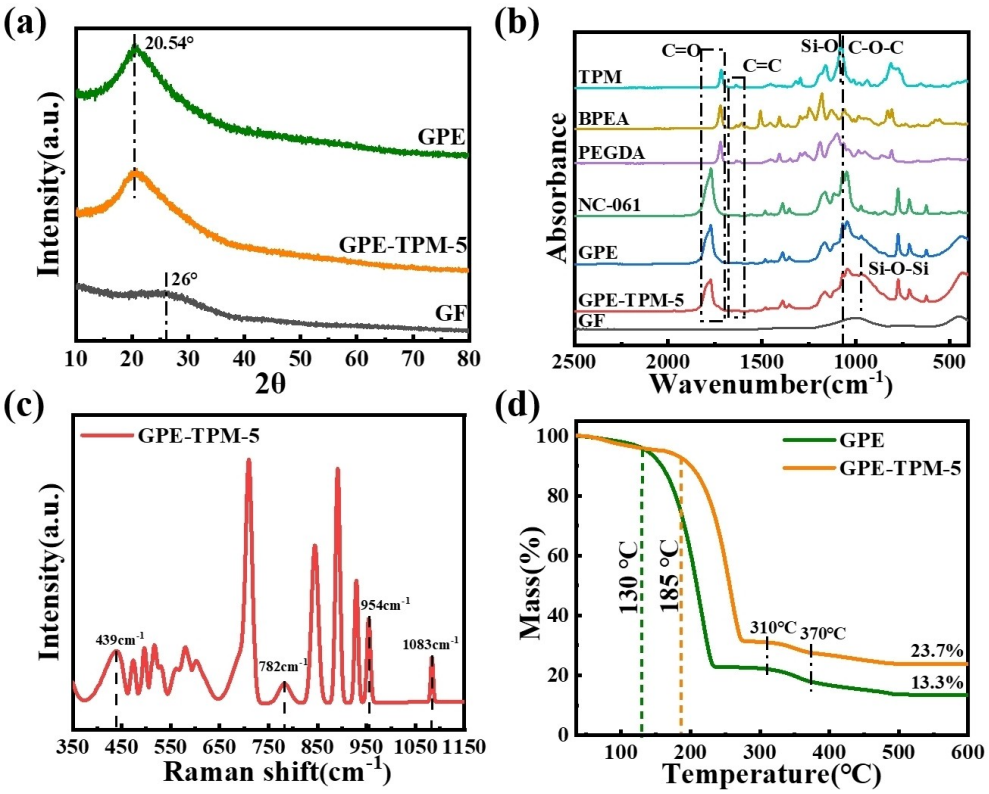

Figure 3. (a) XRD patterns; (b) FTIR spectra of TPM, BPEA, PEGDA, LE, GPE, GPE-TPM-5 and GF at 2500~400 cm^{-1}; (c) Raman spectra of GPE-TPM-5; (d) TGA curves of GPE and GPE-TPM-5.

Research Article
doi.org/10.1002/batt.202500066
Chemistry Europe
European Chemical Societies Publishing

ization, the residual mass of GPE-TPM-5 remains above 20%, whereas that of GPE is approximately 13%. This difference can be attributed to the incorporation of TPM, which enhances the complexity of the polymer crosslinking network and effectively suppresses the degradation of LE at elevated temperatures. Consequently, GPE-TPM-5 exhibits superior high-temperature resistance and significantly improves the thermal stability of SMB, a critical factor for battery safety.

The ionic conductivity of GPEs with varying amounts of TPM was evaluated over a temperature range of 30~90 °C, as shown in Figure 4a. The results indicate that the addition of TPM significantly enhances the conductivity. Specifically, GPE-TPM-5 exhibited the highest conductivity within the tested temperature range, reaching 4.54×10^{-2} S cm^{-1} at 30 °C (close to room temperature) and 1.06×10^{-1} S cm^{-1} at 90 °C. In contrast, the GPE showed lower conductivity values of 4.84×10^{-3} S cm^{-1} and 1.05×10^{-2} S cm^{-1} at the same temperatures, respectively. Notably, the conductivity of GPE-TPM-10 decreased to 3.61×10^{-2} S cm^{-1} at 30 °C, which can be attributed to the increased rigidity of the polymer chains. Repeated tests confirmed that the conductivity of GPE-TPM-5 remains stable within a narrow range (Figure S2).

EIS testing was employed to conduct the NVP||Na batteries prior to charging and discharging cycles (Figure 4b, c). The electrochemical impedance spectrum comprises a semicircle and a straight line. The intersection point of the semicircle in the ultra-high frequency region represents the bulk resistance (R_s) of the battery, while the magnitude of the semicircle corresponds to the charge transfer resistance (R_{ct}), which is associated with impedance arising from charge transport

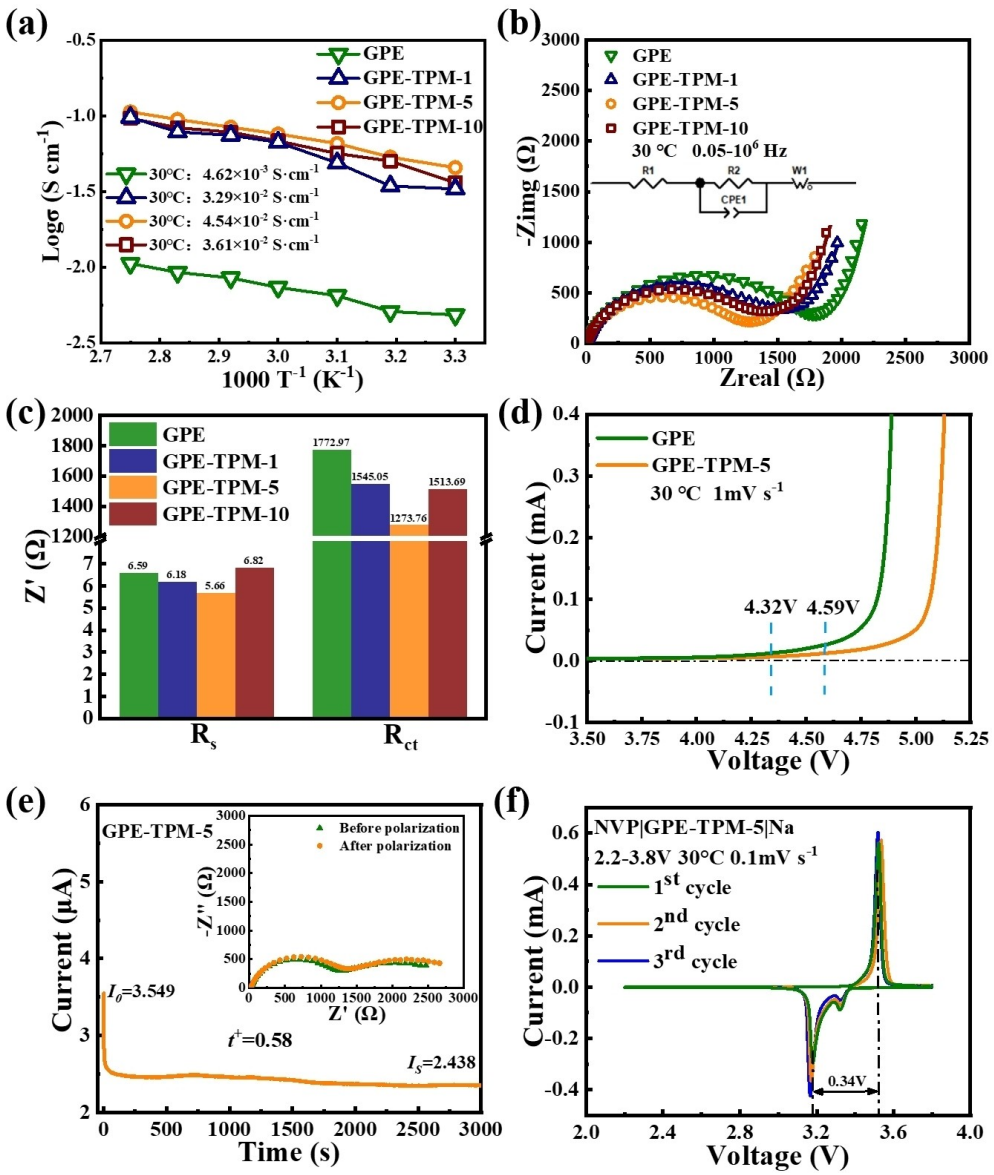

Figure 4. (a) The ionic conductivity of GPE, GPE-TPM-1, GPE-TPM-5 and GPE-TPM-10; (b) EIS curves and (c) R_s and R_{ct} values of NVP|GPE|Na, NVP|GPE-TPM-1|Na, NVP|GPE-TPM-5|Na, and NVP|GPE-TPM-10|Na battery; (d) LSV curves of GPE and GPE-TPM-5; (e) Current density and EIS curves of Na|GPE-TPM-5|Na battery before and after polarization. (f) CV curves of NVP|GPE-TPM-5|Na battery.

through the surface layer and the interfacial charge transfer process.[45] The equivalent circuit model used for fitting EIS tests has been shown in Figure 4b. R_1 (R_s)is the total ohmic impedance, CPE_1 is the constant phase element related to the double layer capacity, R_2 (R_{ct})is the charge-transfer impedance of the electrodes and W_1 is the generalized finite Warburg impedance (Z_w). It is evident that the R_s value remains nearly constant and the R_{ct} value exhibits a significant decrease following the incorporation of TPM, indicating that the introduction of siloxane groups into the polymer network does not appreciably alter the polymer's resistance. The decrease in R_{ct} can be attributed to the reduced viscosity of the electrolyte, as the rotational energy of the Si–O bond is only 3.3 kJ mol^{-1}, significantly lower than the 13.8 kJ mol^{-1} of the C–C bond.[46] The lower rotational energy imparts greater flexibility to the polymer chain segments, the increased flexibility of the chain segments promotes ion transport within the electrolyte, thereby improving both conductivity and ion transport efficiency. The increase in R_{ct} of GPE-TPM-10 can be attributed to the higher TPM content, which leads to the formation of additional Si–O–Si bonds. This may enhance the crystallinity and rigidity of the polymer. These findings are consistent with the XRD test results. Increased crystallinity and rigidity hinder the chain segment mobility, thereby reducing the polymer's ability to transfer electrical charge.[18]

Figure 4d shows the LSV curves of GPE and GPE-TPM-5. A scanning rate of 1 mV s^{-1} was employed, which allows for more precise determination of oxidation stability. The electrochemical stability window of the electrolyte is defined by its oxidation potential. Test results indicate that the initial oxidation potential of GPE is 4.32 V, while that of GPE-TPM-5 increases to 4.59 V, demonstrating a broader electrochemical stability window. The enhanced oxidative stability can be attributed to two key factors: On one hand, the Si–O bond energy (460 kJ mol^{-1}) is significantly higher than that of the C–C bond (347 kJ mol^{-1}).[47] On the other hand, the substantial difference in electronegativity between Si and O results in a polar Si–O bond, which is more stable compared to the non-polar C–C bond.

GPE-TPM-5 and GPE were individually assembled into sodium symmetric batteries to conduct the ion migration number test. The results are presented in Figure 4e and S3. GPE-TPM-5 demonstrated an excellent sodium-ion transference number (t_{Na^+}) of 0.58, which represents a significant improvement over the t_{Na^+} of 0.38 observed for GPE. Obviously, the addition of TPM effectively increased the t_{Na^+} of polymer electrolyte. The presence of a substantial number of ester groups in GPE that facilitate sodium salt dissociation, however, as indicated by the aforementioned analysis, GPE-TPM-5 contains the softer polymer chain segments, and the movement of chain segment is the main means of Na^+ migration in the polymer electrolyte. Therefore, softer polymer chain means that Na^+ migration is more efficient. Previous research has demonstrated that high ion transference number can reduce concentration polarization, which is essential for enhancing the long-term cyclic stability of batteries.[48]

NVP|GPE-TPM-5|Na and NVP|GPE|Na batteries were assembled and underwent CV testing within a voltage range of 2.2~3.8 V at a scanning rate of 0.1 mV s^{-1}. The CV curve is presented in Figure 4f. The CV curve of NVP|GPE-TPM-5|Na battery exhibits excellent repeatability and reversibility, which can be attributed to its high conductivity and t_{Na^+} of GPE-TPM-5.[49] The potential difference between the oxidation peak and the reduction peak is merely 0.34 V, indicating a low degree of electrode polarization. The narrower and more rapid voltammetric response signifies faster kinetics. The observed oxidation peak at 3.52 V and two distinct reduction peaks at 3.18 V and 3.32 V can be ascribed to the de-intercalation/intercalation of Na^+ as a result of the V^{4+}/V^{3+} redox reaction.[50] In particular, the small irreversible reduction peak observed at 3.32 V exhibits a decreasing peak current with increasing cycling. This phenomenon is potentially associated with the structural rearrangement that occurs during the transfer of Na^+ from the Na(1) to the Na(2).[51] The current intensities of the oxidation peak (3.52 V) and the reduction peak (3.18 V) in the third cycle are 0.60 and 0.42 mA, respectively. In contrast, these current intensities for the oxidation peak and the reduction peak in GPE are 0.46 and 0.28 mA (Figure S4). The redox peak of NVP|GPE-TPM-5|Na battery is sharper and more intense, which indicates that the addition of TPM can suggest a facile Na^+ insertion/extraction process, lead to a higher electrochemical reaction rate and improve reaction kinetics in battery.

The electrochemical stability of GPE and GPE-TPM-5 with sodium anodes was evaluated using sodium symmetrical batteries. The results (Figure 5a, b) indicate that at a current density of 0.1 mA cm^{-2}, Na|GPE-TPM-5|Na battery can maintain stable cycling for over 3000 h, whereas Na|GPE|Na battery experiences complete short-circuiting within less than 1300 h. It is observed that the polarization voltage of Na|GPE-TPM-5|Na battery stabilizes at approximately 100 mV after cycling, while that of Na|GPE|Na battery exceeds 200 mV. This is due to the GPE-TPM-5 with high conductivity and ion transference number, which provides a fast transport channel for Na^+ and guides its uniform distribution and deposition.[52–54] When the current density is increased to 0.25 mA cm^{-2}, the voltage during the Na|GPE|Na battery operation exceeds 150 mV, with a rapid increase starting after 250 h. In contrast, the voltage during the Na|GPE-TPM-5|Na battery operation remains stable at around 90 mV until approximately 1250 h, after which it gradually increases. These findings demonstrate that GPE-TPM-5 exhibits superior inhibition of sodium dendrite formation.

The SEM images of the surface of sodium metal anode after 500 h cycling test of the sodium symmetrical batteries are presented in Figure 5c. The surface morphology of the sodium with GPE exhibits significant unevenness, accompanied by numerous defects and damaged regions. In contrast, the sodium surface with GPE-TPM-5 demonstrates a notably dense and smooth structure. EDS analysis was performed on both samples. It is evident that the addition of TPM resulted in a substantial increase in Cl content from 0.1% to 5.6%, and F content from 1.3% to 8.3% (Figure S5). This indicates the formation of a SEI film enriched with F and Cl compounds on the sodium surface. The SEI interface, which incorporates two halides, not only facilitates ion diffusion at the interface and effectively inhibits the formation of sodium dendrites, but also

Research Article
doi.org/10.1002/batt.202500066
Chemistry Europe
European Chemical Societies Publishing

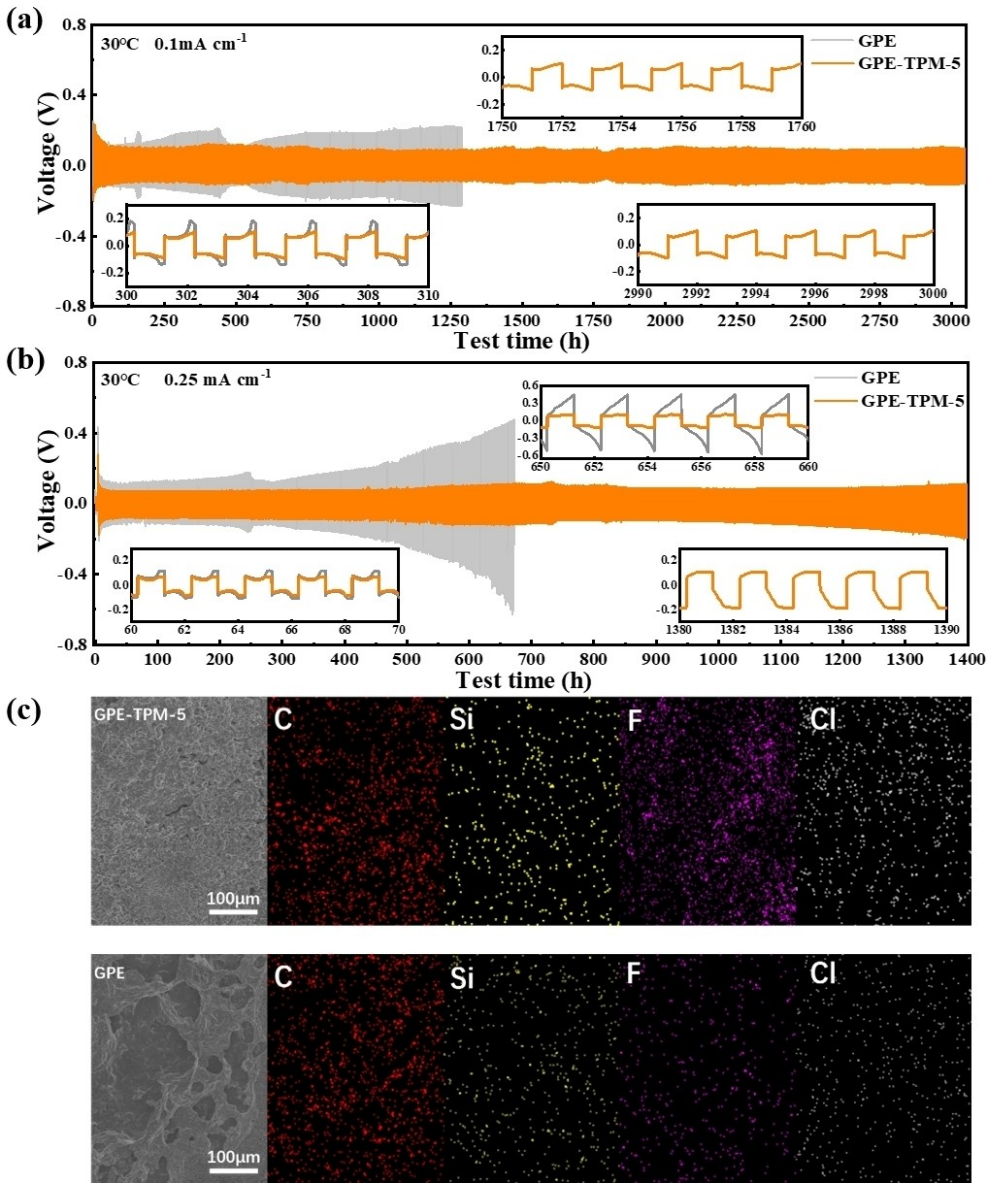

Figure 5. Cycling performance of sodium symmetric batteries at (a) 0.1 mAh cm^{-2} and (b) 0.25 mAh cm^{-2}; (c) SEM images and EDS mappings of the surface of Na in NVP|GPE-TPM-5|Na and NVP|GPE|Na battery after 500 h cycling test.

mitigates the side reactions between the electrode and the interface under high voltage conditions.[55,56] Furthermore, the elevated Si content may suggest the presence of organic components derived from polysiloxane within the SEI. Previous research has demonstrated that the high flexibility and modulus of polysiloxane can effectively suppress dendrite formation on the metal surface.[57,58] On the other hand, whether the polysiloxane is in the electrolyte or in the SEI, its high flexibility is conducive to adapting to the volumetric expansion of Na deposition.[59,60] The above phenomena explain the results observed in the symmetric batteries cycle testing, the incorporation of TPM enhances the cycling life of batteries and improves its interfacial stability.

We also conducted EIS tests on NVP|GPE-TPM-5|Na batteries both before and after charge-discharge cycles. The equivalent circuit model used for fitting EIS before charge and discharge is the same as that in Figure 4b, and the equivalent circuit model used for fitting EIS after charge and discharge is shown in Figure S6a, where CPE_1 and CPE_2 are the constant phase element, related to the SEI film capacity and the double layer capacity, respectively. R_2 (R_{sei}) represents the resistance of the SEI film and R_3 (R_{ct}) is the charge-transfer impedance of the electrodes. By observing the change of resistance, the overall impedance of NVP|GPE-TPM-5|Na batteries showed a decreasing trend during the cycle and tended to be stable after 10 cycles. Figure S6b shows the changes of R_s, R_{sei} and R_{ct} of NVP|GPE-TPM-5|Na batteries, both of R_s and R_{ct} show a downward trend on the whole while R_{sei} shows an upward trend, and gradually maintain stability at last. These findings are consistent with the EIS test results. The increase in R_{sei} suggests the

Research Article
doi.org/10.1002/batt.202500066
Chemistry Europe
European Chemical Societies Publishing

formation of a SEI film at the electrode/electrolyte interface during cycling, while the decrease of R_{ct} means that the SEI film improves the reaction kinetics and speeds up the transport efficiency of ions at the electrode/electrolyte interface, which is beneficial for the rate performance and long-term cycle performance of the NVP|GPE-TPM-5|Na batteries.

NVP|GPE-TPM-5|Na and NVP|GPE|Na batteries were evaluated in a voltage range of 2.2~3.8 V. The results are shown in Figure 6a. At a rate of 0.5 C, the discharge specific capacity of NVP|GPE-TPM-5|Na battery is measured at 99.6 mAh g^{-1}, marginally surpassing that of NVP|GPE|Na battery at 97.9 mAh g^{-1}. When the rate increases to 5 C, the specific capacity of NVP|GPE-TPM-5|Na battery decreases to 92.7 mAh g^{-1}. Notably, even at an elevated rate of 50 C, the specific capacity of NVP|GPE-TPM-5|Na battery remains at 76.6 mAh g^{-1}. Under various current density conditions, the discharge capacity of NVP|GPE-TPM-5|Na battery exceeds that of NVP|GPE|Na battery, indicating that the incorporation of

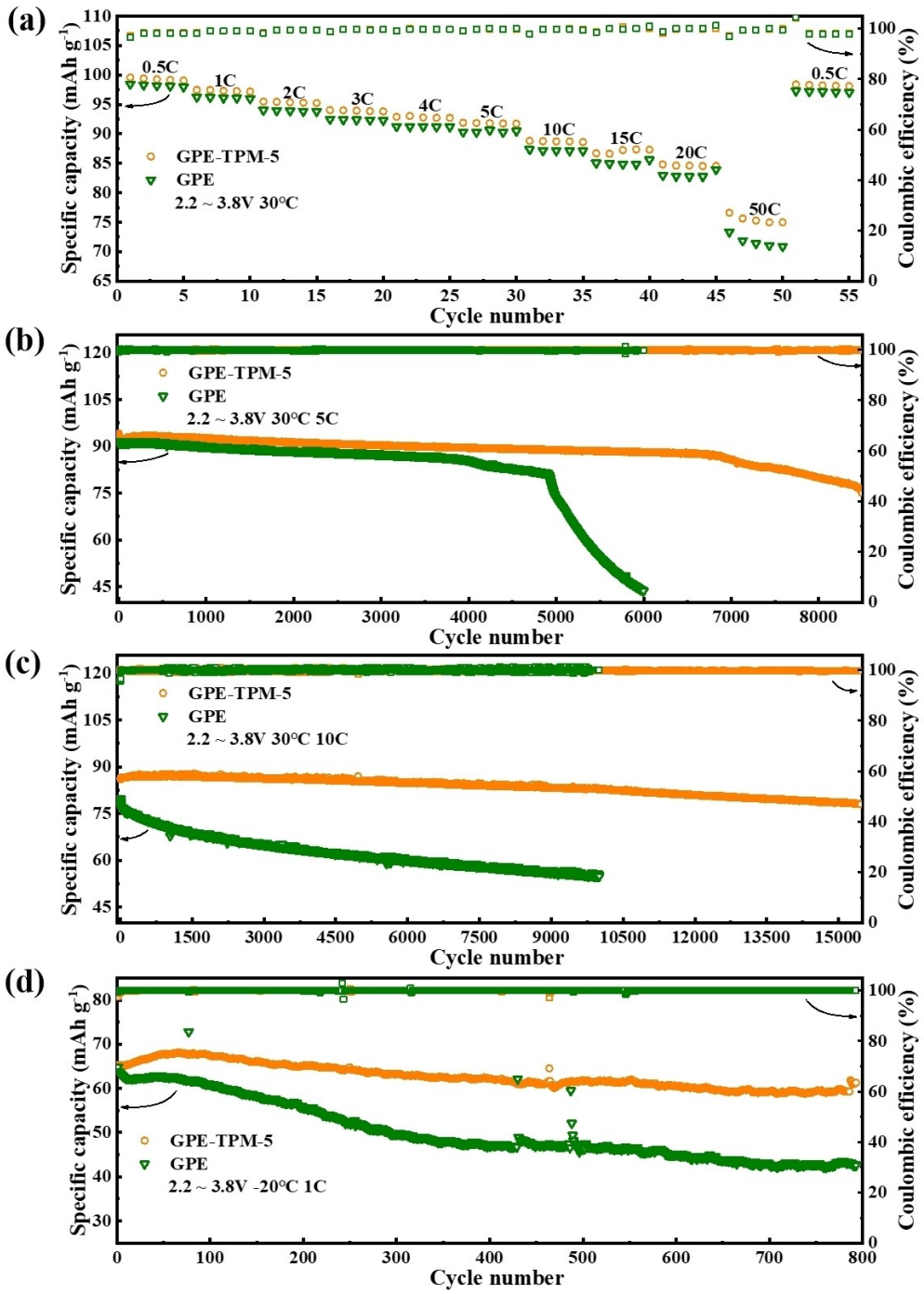

Figure 6. (a) Rate performance of NVP|GPE|Na and NVP|GPE-TPM-5|Na battery. Long-term cycling performance of NVP|GPE|Na and NVP|GPE-TPM-5|Na battery at (b) 5 C at 30 °C, (c) 10 C at 30 °C and (d) 1C at −20 °C.

TPM enhances the discharge capacity, particularly under high current densities. Upon restoring the rate to 0.5 C, the capacity of NVP|GPE-TPM-5|Na battery stabilizes at 98.4 mAh g^{-1}. The results show that the system exhibits superior rate performance.

The long-term cycling tests were conducted at 5 C and 10 C, and are displayed in Figure 6b, c, respectively. NVP|GPE-TPM-5|Na battery demonstrates remarkable stability. At a 5 C rate, the initial capacity is 94.1 mAh g^{-1}, with a decline in capacity observed after approximately 7000 cycles. After 8000 cycles, the capacity of NVP|GPE-TPM-5|Na battery retention rate remains at 85% (79.9 mAh g^{-1}). At 10 C, the initial capacity of NVP|GPE-TPM-5|Na battery is 86.1 mAh g^{-1}, enabling NVP to operate stably for over 15000 cycles, with a final capacity of 78.6 mAh g^{-1} and a retention rate as high as 91%. Although the initial capacity of NVP|GPE|Na battery being comparable to that of NVP|GPE-TPM-5|Na battery at 5 C, the capacity of NVP|GPE|Na battery begins to decline rapidly after fewer than 5000 stable cycles. After 6000 cycles, the capacity of NVP|GPE|Na battery has diminished to 43.6 mAh g^{-1}. The initial capacity of NVP|GPE|Na battery is 79.7 mAh g^{-1} at 10 C, exhibiting a rapid decline in capacity during the early stages of cycling. After 10000 cycles, NVP|GPE|Na battery only remains 63.3% of the initial capacity. In Figure S4a, b, it can be seen that the overpotential of NVP|GPE-TPM-5|Na battery does not increase significantly after extensive cycling at both 5 C and 10 C.

The cyclic performance of NVP|GPE-TPM-5|Na battery was evaluated at −20 °C and 1C, as illustrated in Figure 6d. Initially, the NVP|GPE-TPM-5|Na battery exhibits an increase of capacity. This phenomenon can be attributed to the sluggish movement of polymer chain segments and reduced ion transport kinetics at low temperature. Therefore, to achieve internal stabilization, the batteries require a prolonged activation period. The charge-discharge curve (Figure S7c) of NVP|GPE-TPM-5|Na battery indicates a higher overpotential during the first cycle, along with the presence of two charging plateaus. However, even at a low temperature, NVP|GPE-TPM-5|Na battery exhibited a capacity of 67.9 mAh g^{-1}, with a capacity retention rate of 94% (61.3 mAh·g^{-1}) after 800 cycles. In contrast, only 42.6 mAh g^{-1} remained after 800 cycles for NVP|GPE|Na battery. This phenomenon can be attributed to the enhanced flexibility imparted by TPM to the polymer chain segments, which enables effective Na^+ transfer even in low-temperature working environments,[19] thereby endowing NVP|GPE-TPM-5|Na battery with excellent low-temperature performance.

3. Conclusions

In summary, a gel polymer electrolyte with high ionic conductivity and t_{Na^+} was successfully synthesized through grafting the siloxane groups. The increased flexibility of the polymer chain segments, attributed to the low rotational energy of Si–O bonds, facilitates the transport efficiency of Na^+. Consequently, the conductivity of GPE-TPM-5 and t_{Na^+} at 30 °C are 4.54×10^{-2} S cm^{-1} and 0.58, respectively. Furthermore, the higher bond energy of Si–O compared to C–C enables GPE to possess a broader electrochemical stability window (4.59 V) and the better thermal stability. The sodium symmetric battery assembled using GPE-TPM-5 can cycle for 3200 h at a current density of 0.1 mA cm^{-2}. The NVP|GPE-TPM-5|Na batteries demonstrate exceptional cycling performance, achieving 15000 cycles at 10 C with capacity retention rates of 91%. Notably, it can still maintain 800 cycles at −20 °C and 1C, delivering a discharge specific capacity of 67.9 mAh g^{-1}. This study provides an innovative strategy for the preparation of gel polymer electrolyte which exhibits excellent long-term cycling performance at high rates and low temperatures.

Acknowledgements

We gratefully acknowledge the financial support from the Ministry of Science and Technology of People's Republic of China (502220178), the Guangdong Basic and Applied Basic Research Foundation (2023A1515110792), and the Researchers Supporting Project Number (RSP2025R304), King Saud University, Riyadh, Saudi Arabia. Additionally, we wish to thank the Analysis and Test Center, Guangdong University of Technology for the microscopy and microanalysis.

Conflict of Interests

The authors declare that they have no known competing financial interests or personal relationships that could have appeared in the work reported in this paper.

Data Availability Statement

The data that support the findings of this study are available from the corresponding author upon reasonable request.

Keywords: In-situ gel polymer electrolyte · siloxane grafted gel polymer electrolyte · sodium metal battery

[1] K. Dai, Y. Zheng, W. Wei, *Adv. Funct. Mater.* **2021**, *31* (13), 2008632, https://doi.org/10.1002/adfm.202008632.
[2] Q. Wang, S. Wang, T. Lu, L. Guan, L. Hou, H. Du, H. Wei, X. Liu, Y. Wei, H. Zhou, *Adv. Sci.* **2023**, *10* (1), 2205233, https://doi.org/10.1002/advs.202205233.
[3] Z. Shen, Y. Cheng, S. Sun, X. Ke, L. Liu, Z. Shi, *Carbon Energy* **2021**, *3* (3), 482–508, https://doi.org/10.1002/cey2.108.
[4] H. Deng, L. Liu, Z. Shi, *Mater. Lett.* **2023**, *340*, 134113, https://doi.org/10.1016/j.matlet.2023.134113.
[5] J. Liang, L. Liu, X. Liu, X. Meng, L. Zeng, J. Liu, J. Li, Z. Shi, Y. Yang, *ACS Appl. Mater. Interfaces* **2021**, *13* (19), 22635–45, https://doi.org/10.1021/acsami.1c04997.
[6] S. Hu, D. Wang, Z. Yuan, H. Zhang, S. Tian, Y. Zhang, B. Zhang, Y. Han, J. Zhang, G. Cui, *Batteries* **2023**, *9* (11), 532, https://doi.org/10.3390/batteries9110532.
[7] J. Yang, M. Zhang, Z. Chen, X. Du, S. Huang, B. Tang, T. Dong, H. Wu, Z. Yu, J. Zhang, G. Cui, *Nano Res.* **2019**, *12* (9), 2230–7, https://doi.org/10.1007/s12274-019-2369-9.
[8] M. Sawicki, L. L. Shaw, *RSC Adv.* **2015**, *5* (65), 53129–54, https://doi.org/10.1039/c5ra08321d.

[9] Y. Zhang, J. Wang, C. Tan, Y. He, Y. Chen, S. Huo, D. Zeng, C. Li, H. Cheng, *J. Membr. Sci.* **2021**, *620*, 118921, https://doi.org/10.1016/j.memsci.2020.118921.
[10] J. Ma, Z. Wang, J. Wu, Z. Gu, X. Xin, X. Yao, *Batteries* **2023**, *9* (1), 28, https://doi.org/10.3390/batteries9010028.
[11] W. Ling, N. Fu, J. Yue, X. X. Zeng, Q. Ma, Q. Deng, Y. Xiao, L. J. Wan, Y. G. Guo, X. W. Wu, *Adv. Energy Mater.* **2020**, *10* (9), 1903966, https://doi.org/10.1002/aenm.201903966.
[12] J. Huang, Z. Shen, S. J. Robertson, Y. Lin, J. Zhu, K. Yang, Y. Wang, M. Shao, Z. Shi, *Chem. Eng. J.* **2023**, *475*, 145802, https://doi.org/10.1016/j.cej.2023.145802.
[13] P. Ding, Z. Lin, X. Guo, L. Wu, Y. Wang, H. Guo, L. Li, H. Yu, *Mater Today (Kidlington)* **2021**, *51*, 449–74, https://doi.org/10.1016/j.mattod.2021.08.005.
[14] C. Simari, E. Lufrano, L. Coppola, I. Nicotera, *Membranes (Basel)* **2018**, *8* (3), 69, https://doi.org/10.3390/membranes8030069.
[15] Y. Lin, J. Chen, J. Zhu, J. Zhong, K. Yang, H. Deng, J. Huang, Z. Shen, Z. Shi, *Surf Interfaces* **2023**, *37*, 102737, https://doi.org/10.1016/j.surfin.2023.102737.
[16] T. Liu, J. Zhang, W. Han, J. Zhang, G. Ding, S. Dong, G. Cui, *J. Electrochem. Soc.* **2020**, *167 (7)*, 70527, https://doi.org/10.1149/1945-7111/ab76a4.
[17] C. Fu, M. Iacob, Y. Sheima, C. Battaglia, L. Duchêne, L. Seidl, D. M. Opris, A. Remhof, *J. Mater. Chem. A* **2021**, *9* (19), 11794–801, https://doi.org/10.1039/D1TA02689E.
[18] X. He, J. Lin, G. Ge, F. Yan, K. Zhu, B. Shen, J. Zhai, *J. Power Sources* **2023**, *555*, 232346, https://doi.org/10.1016/j.jpowsour.2022.232346.
[19] H. P. Liang, M. Zarrabeitia, Z. Chen, S. Jovanovic, S. Merz, J. Granwehr, S. Passerini, D. Bresser, *Adv. Energy Mater.* **2022**, *12* (16), 2200013, https://doi.org/10.1002/aenm.202200013.
[20] X. Zhou, Z. Li, W. Li, X. Li, J. Fu, L. Wei, H. Yang, X. Guo, *Adv. Funct. Mater.* **2023**, *33* (11), 2212866, https://doi.org/10.1002/adfm.202212866.
[21] B. A. S. K. Vidyanand Vijayakumar, *Energy Environ. Sci.* **2021**, *14*, 2708–88, https://doi.org/10.1039/d0ee03527k.
[22] X. Zhou, X. Li, Z. Li, H. Xie, J. Fu, L. Wei, H. Yang, X. Guo, *J. Mater. Chem. A* **2021**, *9* (34), 18239–46, https://doi.org/10.1039/D1TA04631D.
[23] P. Y. Ji, J. Fang, Y. Y. Zhang, P. Zhang, J. B. Zhao, *ChemElectroChem* **2017**, *4* (9), 2352–8, https://doi.org/10.1002/celc.201700256.
[24] G. Xi, M. Xiao, S. Wang, D. Han, Y. Li, Y. Meng, *Adv. Funct. Mater.* **2021**, *31* (9), 2007598, https://doi.org/10.1002/adfm.202007598.
[25] Z. Shen, H. Wen, H. Zhou, L. Hao, H. Chen, X. Zhou, *Mater. Sci. Eng. C* **2019**, *105*, 110073, https://doi.org/10.1016/j.msec.2019.110073.
[26] M. J. Sever, J. T. Weisser, J. Monahan, S. Srinivasan, J. J. Wilker, *Angew. Chem. Int. Ed.* **2004**, *43* (4), 448–50, https://doi.org/10.1002/anie.200352759.
[27] X. Zhang, F. Shen, X. Long, S. Zheng, Z. Ruan, Y. Cai, X. Hong, Q. Zheng, *Energy Storage Mater.* **2022**, *52*, 201–9, https://doi.org/10.1016/j.ensm.2022.07.045.
[28] C. Li, Y. Huang, X. Liu, C. Chen, X. Feng, Z. Zhang, P. Liu, *Mater. Chem. Front.* **2022**, *6* (12), 1672–80, https://doi.org/10.1039/D1QM01589 C.
[29] J. Zheng, Y. Yang, W. Li, X. Feng, W. Chen, Y. Zhao, *J. Mater. Chem. A* **2020**, *8* (43), 22962–8, https://doi.org/10.1039/D0TA09490 K.
[30] Y. Lin, Z. Shen, J. Huang, J. Zhu, S. Jiang, S. Zhan, Y. Xie, J. Chen, Z. Shi, *J. Power Sources* **2023**, *584*, 233612, https://doi.org/10.1016/j.jpowsour.2023.233612.
[31] D. Zhang, Z. Liu, Y. Wu, S. Ji, Z. Yuan, J. Liu, M. Zhu, *Adv. Sci.* **2022**, *9* (12), 2104277, https://doi.org/10.1002/advs.202104277.
[32] Z. Wang, H. Ma, B. S. Hsiao, B. Chu, *Polymer (Guildf)* **2014**, *55* (1), 366–72, https://doi.org/10.1016/j.polymer.2013.10.049.
[33] W. Cao, J. Lu, K. Zhou, G. Sun, J. Zheng, Z. Geng, H. Li, *Nano Energy* **2022**, *95*, 106983, https://doi.org/10.1016/j.nanoen.2022.106983.
[34] H. Wang, Q. Wang, X. Cao, Y. He, K. Wu, J. Yang, H. Zhou, W. Liu, X. Sun, *Adv. Mater.* **2020**, *32* (37), 2001259, https://doi.org/10.1002/adma.202001259.
[35] L. Zhou, H. Zhao, K. Liang, J. Chen, J. Li, X. Huang, Y. Qi, Y. Ren, *J. Colloid Interface Sci.* **2022**, *613*, 606–15, https://doi.org/10.1016/j.jcis.2021.12.147.
[36] J. Hao, M. Gong, Y. Wu, C. Wu, J. Luo, T. Xu, *J. Hazard. Mater.* **2013**, *244–245*, 348–56, https://doi.org/10.1016/j.jhazmat.2012.11.056.
[37] A. Jelić, M. Sekulić, M. Travica, J. Gržetić, V. Ugrinović, A. D. Marinković, A. Božić, M. Stamenović, S. Putić, *Polymers (Basel).* **2022**, *14* (6), 1255, https://doi.org/10.3390/polym14061255.
[38] J. T. Kloprogge, R. L. Frost, *Spectrochim. Acta Part A* **2000**, *56* (3), 501–13, https://doi.org/10.1016/S1386-1425(99)00141–9.
[39] E. L. Lee, I. E. Wachs, *J. Phys. Chem. C* **2007**, *111* (39), 14410–25, https://doi.org/10.1021/jp0735482.
[40] S. Lwin, Y. Li, A. I. Frenkel, I. E. Wachs, *ACS Catal.* **2016**, *6* (5), 3061–71, https://doi.org/10.1021/acscatal.6b00389.
[41] A. Alessi, S. Agnello, G. Buscarino, F. M. Gelardi, *J. Non-Cryst. Solids* **2013**, *362*, 20–4, https://doi.org/10.1016/j.jnoncrysol.2012.11.006.
[42] S. Almuhamed, M. Bonne, N. Khenoussi, J. Brendle, L. Schacher, B. Lebeau, D. C. Adolphe, *J. Ind. Eng. Chem.* **2016**, *35*, 146–52, https://doi.org/10.1016/j.jiec.2015.12.024.
[43] Z. Shen, J. Zhong, S. Jiang, W. Xie, S. Zhan, K. Lin, L. Zeng, H. Hu, G. Lin, Y. Lin, S. Sun, Z. Shi, *ACS Appl. Mater. Interfaces* **2022**, *14* (36), 41022–36, https://doi.org/10.1021/acsami.2c11397.
[44] C. Tsao, C. Wang, E. Trevisanello, F. H. Richter, D. Kuo, J. Janek, C. Chang, H. Teng, P. Kuo, *ACS Appl. Energ. Mater.* **2023**, *6* (11), 5662–70, https://doi.org/10.1021/acsaem.2c03892.
[45] C. Dong, Z. Lin, Y. Yin, Y. Qiao, W. Wang, Q. Wu, C. Yang, D. Rooney, C. Fan, K. Sun, *J. Energy Chem.* **2021**, *55*, 1–9, https://doi.org/10.1016/j.jechem.2020.06.060.
[46] F. Weinhold, R. West, *Organometallics* **2011**, *30* (21), 5815–24, https://doi.org/10.1021/om200675d.
[47] J. Yu, K. Wang, W. Song, H. Huang, C. Liang, Y. Xia, J. Zhang, Y. Gan, F. Wang, W. Zhang, *Chem. Eng. J.* **2021**, *406*, 126805, https://doi.org/10.1016/j.cej.2020.126805.
[48] Z. Shen, J. Zhong, W. Xie, J. Chen, X. Ke, J. Ma, Z. Shi, *Acta Metall. Sin. (Engl. Lett.)* **2021**, *34* (3), 359–72, https://doi.org/10.1007/s40195-021-01191-8.
[49] S. Yang, Q. Fan, Z. Shi, L. Liu, J. Liu, X. Ke, J. Liu, C. Hong, Y. Yang, Z. Guo, *ACS Appl. Mater. Interfaces* **2019**, *11* (40), 36742–50, https://doi.org/10.1021/acsami.9b12578.
[50] S. Y. Lim, H. Kim, R. A. Shakoor, Y. Jung, J. W. Choi, *J. Electrochem. Soc.* **2012**, *159* (9), A1393–7, https://doi.org/10.1149/2.015209jes.
[51] X. Jiang, L. Yang, B. Ding, B. Qu, G. Ji, J. Y. Lee, *J. Mater. Chem. A* **2016**, *4* (38), 14669–74, https://doi.org/10.1039/C6TA05030 A.
[52] L. Wang, S. Xu, Z. Wang, E. Yang, W. Jiang, S. Zhang, X. Jian, F. Hu, *Escience* **2023**, *3* (2), 100090, https://doi.org/10.1016/j.esci.2022.100090.
[53] X. Xie, L. Wei, J. Lu, A. Xu, B. Wang, X. Xiao, A. Wang, Z. Jin, Z. Shi, W. Wang, *Energy Storage Mater* **2024**, *67*, 103323, https://doi.org/10.1016/j.ensm.2024.103323.
[54] H. Shi, J. Zheng, T. Wan, H. Wang, Z. Wen, F. Zheng, M. Su, A. Dou, Y. Zhou, A. Naveed, P. Zhang, H. Wang, R. Guo, Y. Liu, D. Chu, *J. Energy Chem.* **2025**, *101*, 392–401, https://doi.org/10.1016/j.jechem.2024.09.056.
[55] A. Sun, H. Tu, Z. Sun, Z. He, Y. Wang, J. Wang, Y. Zheng, F. Zhu, L. Wang, F. Mushtaq, P. Xue, J. Liu, M. Liu, *ACS Energy Lett.* **2024**, *9* (6), 2545–53, https://doi.org/10.1021/acsenergylett.4c00548.
[56] X. Xie, J. Chen, X. Chen, Z. Shi, *J Electroanal Chem (Lausanne)* **2023**, *949*, 117862, https://doi.org/10.1016/j.jelechem.2023.117862.
[57] F. Liu, Q. Xiao, H. B. Wu, L. Shen, D. Xu, M. Cai, Y. Lu, *Adv. Energy Mater.* **2018**, *8* (6), 1701744, https://doi.org/10.1002/aenm.201701744.
[58] J. Meng, F. Chu, J. Hu, C. Li, *Adv. Funct. Mater.* **2019**, *29* (30), 1902220, https://doi.org/10.1002/adfm.201902220.
[59] B. Zhu, Y. Jin, X. Hu, Q. Zheng, S. Zhang, Q. Wang, J. Zhu, *Adv. Mater.* **2017**, *29* (2), 1603755, https://doi.org/10.1002/adma.201603755.
[60] Z. Shen, J. Zhong, J. Chen, W. Xie, K. Yang, Y. Lin, J. Chen, Z. Shi, *Chin. Chem. Lett.* **2023**, *34* (3), 107370, https://doi.org/10.1016/j.cclet.2022.03.093.

Manuscript received: January 28, 2025
Revised manuscript received: February 24, 2025
Accepted manuscript online: February 26, 2025
Version of record online: March 13, 2025